

See discussions, stats, and author profiles for this publication at: <https://www.researchgate.net/publication/38039664>

Heterogeneous Ultrathin Films of Poly(vinyl alcohol)/Layered Double Hydroxide and Montmorillonite Nanosheets via Layer-by-Layer Assembly

ARTICLE *in* THE JOURNAL OF PHYSICAL CHEMISTRY B · NOVEMBER 2009

Impact Factor: 3.3 · DOI: 10.1021/jp907784k · Source: PubMed

CITATIONS

52

READS

66

6 AUTHORS, INCLUDING:



[Shu Huang](#)

KTH Royal Institute of Technology

32 PUBLICATIONS 805 CITATIONS

[SEE PROFILE](#)



[Tianxi Liu](#)

Fudan University

232 PUBLICATIONS 7,176 CITATIONS

[SEE PROFILE](#)

Heterogeneous Ultrathin Films of Poly(vinyl alcohol)/Layered Double Hydroxide and Montmorillonite Nanosheets via Layer-by-Layer Assembly

Shu Huang, Xi Cen, Hongdan Peng, Shuzhong Guo, Weizhi Wang, and Tianxi Liu*

Key Laboratory of Molecular Engineering of Polymers of Ministry of Education, Department of Macromolecular Science, Laboratory of Advanced Materials, Fudan University, Shanghai 200433, P. R. China

Received: August 12, 2009; Revised Manuscript Received: October 8, 2009

In this paper, Co-Al layered double hydroxide (LDH) and montmorillonite (MMT) have been exfoliated into charged single layers in the solvent of formamide and water, respectively. The structures of individual layers of LDH and MMT were characterized by X-ray diffraction (XRD) and atomic force microscopy (AFM). The delamination mechanisms of LDH and MMT were also discussed. Furthermore, heterogeneous ultrathin films of poly(vinyl alcohol) (PVA)/charged inorganic nanosheets, (PVA/MMT/PVA/LDH)_n, were fabricated by layer-by-layer (LBL) assembly via hydrogen bonding. The LBL assembly process was monitored by UV-vis spectroscopy, and the structures of the heterogeneous ultrathin films were analyzed by XRD.

1. Introduction

Layered double hydroxides (LDH), also known as anionic or hydrotalcite-like clays, are generally expressed as $[M^{2+}_{1-x}M^{3+}_x(OH)_2][A^{n-}_{x/n}\cdot mH_2O]$, where M^{2+} and M^{3+} are divalent and trivalent metal cations respectively, and A is n -valent interlayer guest anion. The positive charge of the layer is generated by the replacement of a portion of divalent metal cation of brucite-like layer with a trivalent cation and is compensated for by the interlayer anions. Recently, LDH has been the subject of intense research due to their potential applications as catalysts and catalyst support,^{1–4} anion exchanger and molecular container,^{5–9} electrical and optical functional materials,^{10–14} flame retardants and nanofillers,^{15–19} and so on.

However, LDH usually stacks together to form a layered structure with a thickness of tens of nanometers due to the strong interlayer electrostatic interactions. In order to have maximum utilization of the LDH layers, much research effort has been devoted to the delamination of LDH into single layers.^{20–22} One of the latest progresses is the successful investigation of the delamination process of LDH by using the microsized hexagonal LDH as precursor and formamide as a delaminating reagent by Sasaki et al. Furthermore, Sasaki et al. obtained LDH/polyelectrolyte ultrathin films by a layer-by-layer (LBL) self-assembly, which has demonstrated exceptional uniformity and versatility for constructing a nanostructure composite with various nano-building blocks.^{23,24} Nevertheless, all the LBL ultrathin LDH/polymer films reported are based on electrostatic force driving assembly, such as [LDH/poly(sodium 4-styrene sulfonate)]_n and [LDH/sulfonated poly(*p*-phenylene) anionic derivate]_n films.^{23–27}

On the basis of its driving force, LBL assembly can be categorized into several types: electrostatic force, hydrogen bonding, covalent bonding, coordination bonding, and charge transform interaction. The hydrogen-bonded LBL assembly was first introduced by Rubner and Zhang, respectively.^{28,29} After that, various types of polymers with ether, hydroxyl, amino, or carbonyl groups were used to fabricate multilayer nanocomposites via the formation of hydrogen bonding between polymer and inorganic nanomaterials.^{30,31}

Montmorillonite (MMT) has been extensively used in the nanocomposites because it is readily available and has exceptional mechanical properties. The in-plane elastic modulus of MMT has been estimated by Monte Carlo simulations to be ~270 GPa. Kotov et al. fabricated stiff, ultrastrong layered polymer nanocomposites by assembly of a MMT/PVA nanocomposite.^{32,33} Comparing the homogeneous ultrathin films with LDH or MMT, heterogeneous films could probably possess tunable functions due to their structural diversity and combined functionality. In contrast with a negative charged layer of MMT, LDH is a hydrotalcite-like clay with positive charged layer. Therefore, it is impossible to fabricate heterogeneous ultrathin films by alternate assembly of polyelectrolyte and exfoliated LDH and MMT, which act as inorganic building blocks. In the present report, we utilize hydrogen-bonding interaction between polyvinyl alcohol (PVA) and inorganic nanosheets as a driving force to fabricate organic/inorganic multilayer hybrid films in a layer-by-layer manner. Alternative adsorption of PVA and nanolayer results in a uniform growth of films which contain a high concentration of inorganic nanofillers.

2. Experimental Section

2.1. Reagents and Materials. Polyvinyl alcohol (PVA, $M_w = 85\,000–124\,000$, 98–99% hydrolyzed) was purchased from Sigma-Aldrich. Na⁺-Montmorillonite (“Cloisite Na⁺”, MMT) powder was purchased from Southern Clay Products, and 37% HCl, CoCl₂·6H₂O, AlCl₃·6H₂O, NaCl, NaNO₃, and urea were supplied by China Medicine Co. All reactants were of analytical purity and used as received. Ultrapure Milli-Q water was used throughout all the experiments.

2.2. Synthesis of Co-Al-CO₃ LDH and Nitrate-Intercalated LDH. Co-Al LDH used in this study was synthesized on the basis of a previous report with modification.²⁴ First, Co-Al-CO₃ LDH sample was synthesized using a hydrolysis method under hydrothermal conditions. A typical preparation process is described as follows: CoCl₂·6H₂O, AlCl₃·6H₂O, and urea were dissolved in 100 mL of deionized water to give the final concentrations of 10, 5, and 35 mM, respectively. The aqueous mixture was allowed to react in a 100 mL Teflon-lined autoclave at 100 °C for 24 h. After cooling to room temperature, the solid products were filtered, subsequently washed with

* To whom correspondence should be addressed. E-mail: txliu@fudan.edu.cn. Tel: +86-21-55664197. Fax: +86-21-65640293.

deionized water and anhydrous ethanol for several times, and finally air-dried at room temperature. The as-prepared Co-Al-CO₃ LDH was then treated with a NaCl-HCl mixed solution (1 M NaCl and 3.3 mM HCl in 1 L deionized water) for 12 h to complete the decarbonation of LDH and thus to obtain the Co-Al-Cl LDH. The Co-Al-NO₃ LDH was prepared by treating the Cl⁻ intercalated LDH with a conventional anion-exchange process.

2.3. Exfoliation of Co-Al-NO₃ LDH and Na⁺-MMT. LDH/formamide solution was prepared by mixing 200 mL of formamide with 200 mg of Co-Al-NO₃ LDH sample in a flask, which was tightly sealed after purging with nitrogen gas. The mixture was vigorously shaken by a mechanical shaker at a speed of 160 rpm for 2 days. The unexfoliated particles were further removed by centrifugation at 2000 rpm for 10 min. MMT/water suspension was obtained by dissolving 200 mg of clay in 100 cm³ of DI water. After vigorous stirring for 2 weeks, the insoluble fraction was allowed to deposit for 24 h and the suspension was collected for subsequent use.

2.4. Fabrication of Multilayer Films. Quartz slides (1 × 3 cm²) were cleaned in a "piranha" solution (3:1 H₂SO₄:H₂O₂) for 1 h. The cleaned substrates were then thoroughly rinsed with water and dried under nitrogen flow. PVA was dissolved in DI water to get 1 wt % aqueous solution. In a typical LBL assembly preparation, a quartz slide was immersed in 1 wt % solution of PVA for 10 min, rinsed for 1 min with DI water, and gently dried under nitrogen flow for 1 min and subsequently immersed in MMT suspension for 10 min, rinsed for 1 min, and dried with nitrogen for 1 min. This quartz slide was immersed in 1 wt % solution of PVA for 10 min again, followed by water washing and nitrogen drying, which was then dipped into the colloidal suspension of the LDH. The cycle could then be repeated as necessary to obtain the desired number of multilayer of (PVA/MMT/PVA/LDH)_n. For comparison, PVA with exfoliated LDH nanosheet films (PVA/LDH)_n and PVA with exfoliated MMT films (PVA/MMT)_n were assembled with the similar method, respectively.

2.5. Characterizations. A scanning electron microscope (SEM, Tescan 5136 MM) was used to observe the morphology of LDH samples. The SEM samples were coated with gold prior to observation. The Co and Al contents of the LDH samples were measured by inductively coupled plasma (ICP) atomic emission spectroscopy (Hitachi P-4010) after dissolving a weighed amount of sample with an aqueous HCl solution. X-ray diffraction (XRD) patterns of the samples were conducted on an X'Pro X-ray diffractometer with Cu K α radiation ($\lambda = 0.1548$ nm) under a voltage of 40 kV and a current of 40 mA. The atomic force microscopy (AFM) images were acquired in tapping mode by using a Nanoscope IV from Digital Instruments. For AFM observations, the samples were prepared by casting and drying the solution on freshly cleaved mica at room temperature (rt). The FTIR spectra were recorded with a 4 cm⁻¹ spectral resolution on a Nicolet Nexus 470 spectrometer equipped with a DTGS detector by signal-averaging 64 scans. IR samples were in the form of KBr pellets containing 2 wt % predried sample material. UV-vis spectroscopy was carried out on a Perkin-Elmer Lambda 35 UV-vis absorption spectrometer at rt.

3. Results and Discussion

3.1. Structure and Morphology of LDH and Its Exfoliation Behavior. Highly crystalline and monodispersive Co-Al-CO₃ LDH samples were prepared by precipitation through urea hydrolysis approach under hydrothermal condition. Figure 1 shows SEM images of a typical Co-Al-CO₃ LDH

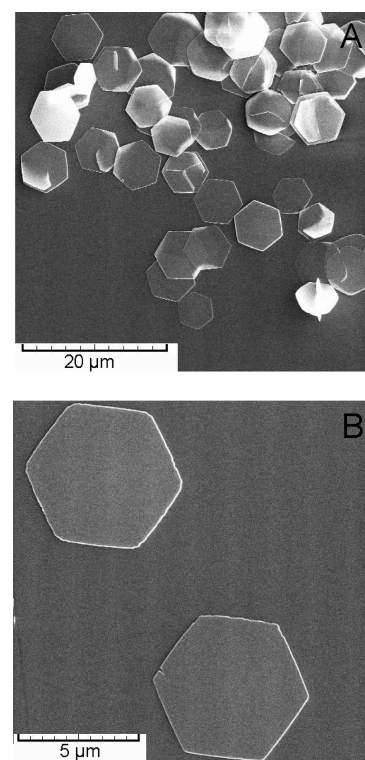


Figure 1. (A) Low and (B) high magnification SEM images of the Co-Al-CO₃ LDH sample.

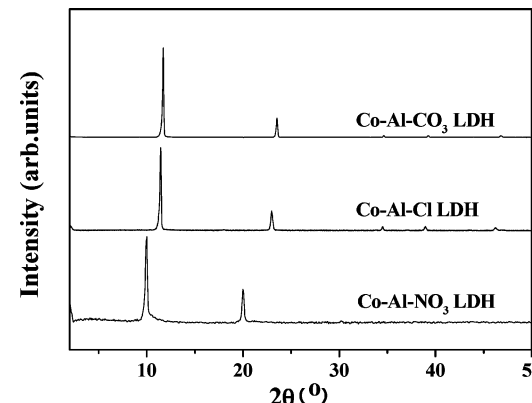


Figure 2. XRD pattern of (a) CO₃²⁻, (b) Cl⁻, (c) NO₃⁻ LDH samples.

sample. As can be seen, the sample consists of uniform and thin hexagonal platelets with a mean lateral size as large as 5 μ m. The molar ratio of Co/Al is determined to be 1.94 by elemental analysis using ICP-AES analysis. The XRD patterns (Figure 2) and FTIR absorption spectra (Figure 3) clearly indicate the high purity of the product. The interlayer CO₃²⁻ must be converted to NO₃⁻, because NO₃⁻ LDH was found to have the best delamination behavior. An effective method based on decarbonation and anion exchange was used to exchange the interlayer CO₃²⁻ into NO₃⁻.²⁴ Figure 2 shows the XRD patterns of the Co-Al-Cl LDH, suggesting that the decarbonation was successfully conducted and that highly crystalline Cl-LDH product was formed. Owing to the incorporation of Cl⁻, the basal spacing of the LDH is increased from 0.75 to 0.78 nm. The SEM image (see Supporting Information, Figure S1) shows that the obtained Co-Al-Cl LDH sample exhibits almost the same morphology and size as the CO₃²⁻ LDH sample, suggesting that no acid corrosion takes place. When being further exchanged by NO₃⁻, the interlayer space of LDH is

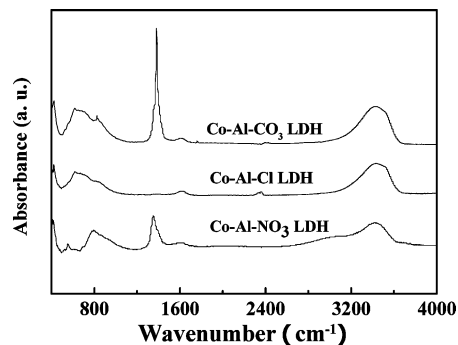


Figure 3. FTIR spectra of (a) CO_3^{2-} , (b) Cl^- , (c) NO_3^- LDH samples.

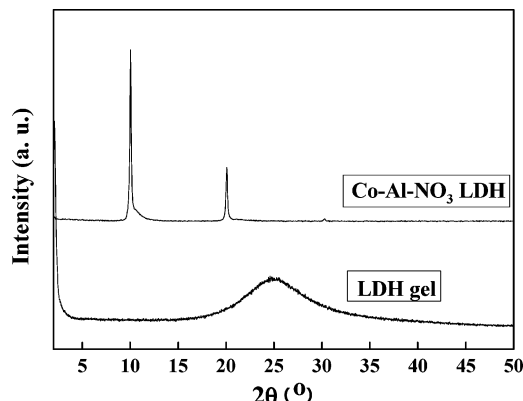


Figure 4. XRD pattern for powdery NO_3^- LDH samples and the colloidal LDH aggregate centrifuged from the suspension.

increased to 0.89 nm. The FTIR spectra of Co-Al- NO_3 LDH also provide evidence about the presence of NO_3^- (absorption band at 1384 cm^{-1}) in the interlayer space. A broad absorption band in a wavenumber range of $3000\text{--}3700\text{ cm}^{-1}$ and absorption around 1630 cm^{-1} are attributed to stretching and bending modes of water existing in the interlayer, respectively.

The as-prepared Co-Al- NO_3 LDH and formamide mixture form an apparently transparent solution after vigorous shaking for 2 days at room temperature. To explore the colloidal state of the LDH sample, the suspension was centrifuged for 20 min at a speed of 30 000 rpm to separate a gel-like aggregate from formamide (solvent). The XRD data for the gel-like LDH sample exhibit a pronounced halo in the range of $2\theta = 20^\circ\text{--}30^\circ$, as depicted in Figure 4, which can be ascribed to the scattering of liquid formamide. One of the most striking features for the paste-like LDH sample is the absence of the sharp basal peaks, which is in contrast to the XRD pattern of powdery LDH sample. This suggests that the host sheets of LDH are almost completely swollen and not in parallel to induce the interference of the X-rays, implying successful exfoliation. The morphology of the exfoliated nanosheets were further examined by AFM. A tapping-mode AFM image (Figure 5) showed two-dimensional ultrathin sheets with lateral dimensions of up to $1\text{ }\mu\text{m}$, although some fragments were also observed in small amounts. Some large nanosheets with lateral dimensions of $>2\text{ }\mu\text{m}$ were occasionally observed. The exfoliated nanosheets were morphologically irregular and dimensionally diminished in comparison with the parent LDH crystallites, indicating the breakage or fracture of sheets during the delamination process. The height profile in Figure 5 revealed that the nanosheets had an average thickness of about 0.9 nm. This value indicated the successful delamination and that the unilamellar LDH or individual LDH platelets were obtained.

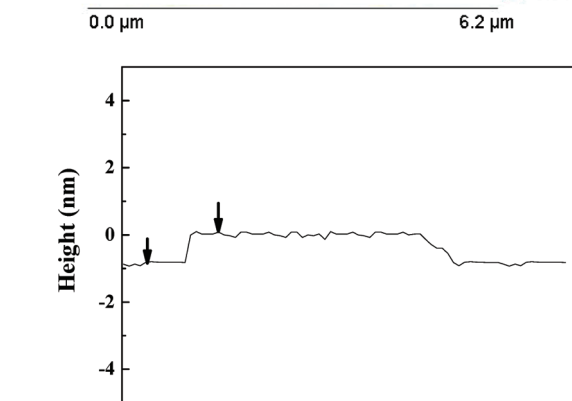
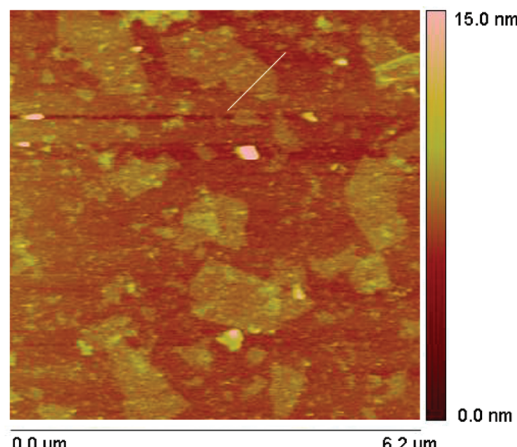


Figure 5. Tapping-mode AFM image of the exfoliated LDH nanosheets deposited on a fresh mica substrate.

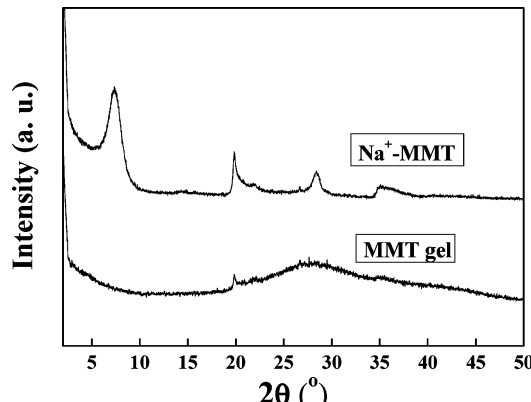


Figure 6. XRD pattern for pristine and the colloidal MMT aggregate centrifuged from the suspension.

3.2. Swelling and Exfoliation Behavior of MMT

Figure 6 shows the XRD patterns of the pristine MMT powder and the colloidal MMT aggregate centrifuged for 10 min from its water suspension at a speed of 10 000 rpm. The (001) basal plane of MMT observed at about 7.23° corresponds to an interlayer spacing of 1.22 nm (calculated from the Bragg equation). Besides, the pristine MMT also showed a distinctive diffraction peak at 19.98° with d -spacing of 0.45 nm, which corresponds to the reflection peak of (020).³⁴ It is interesting to observe that the gel-like MMT sample does not show the (001) basal plane, indicating that MMT had lost its regularity of stacked layers. The main feature for the XRD pattern of the MMT gel sample is the broad halo observed in the 2θ range of $20^\circ\text{--}30^\circ$, due to the scattering of water.³⁵ In addition, a very weak reflection at $2\theta = 19.8^\circ$ is observed, which could be

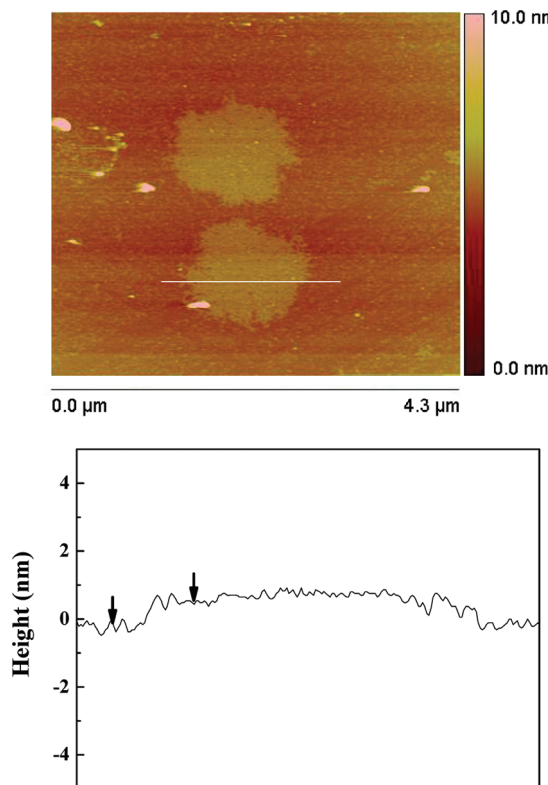


Figure 7. Tapping-mode AFM image of the exfoliated MMT nanosheets deposited on a fresh mica substrate.

assigned to (020) plane for a two-dimensional hexagonal unit cell. This result probably indicates that the two-dimensional crystalline order of the MMT layers was slightly preserved in the colloidal form.³⁴

A tapping-mode AFM image of the MMT gel sample was shown in Figure 7. The height profile scan indicated that the terrace of the flaky crystallites was rather flat. The thickness of the nanosheet was measured to be about 1 nm, clearly demonstrating the nanosheet nature of the gel-like MMT sample, i.e., single MMT platelets. The crystallographic thickness of MMT layer is evaluated to be 0.8 nm based on its atomic architecture. The hydration of the nanosheets may be responsible for the discrepancy between theoretical thickness and the one obtained experimentally.^{35,36}

On the basis of the above results, it is possible to conclude that the delamination of MMT can be achieved in water solution. Without vigorous stirring, the delamination of MMT could not be attained, even when it was immersed in water for 1 month. Clays consist of negatively charged aluminosilicate layers kept together by cations. The most characteristic property of clay is its ability to adsorb water between the layers, resulting in strong repulsive forces and clay expansion. A high degree of interlayer expansion can be achieved by introducing a large volume of water molecules into the interlayer space. The hydrogen bonding between water and MMT interlayer makes the MMT highly swollen, and this highly swollen phase will then exfoliate into single layers with the assistance of mechanical shearing.^{37,38} This delamination process is very similar to those that have been observed for LDH. Thus, this mechanism should commonly exist in other layered systems as well.^{39,40} In fact, our exfoliation experiment was only performed with continuous and vigorous stirring, and it typically took about 2 weeks to achieve complete exfoliation. When stirring was stopped, the mixtures exhibited a clear supernatant solution.

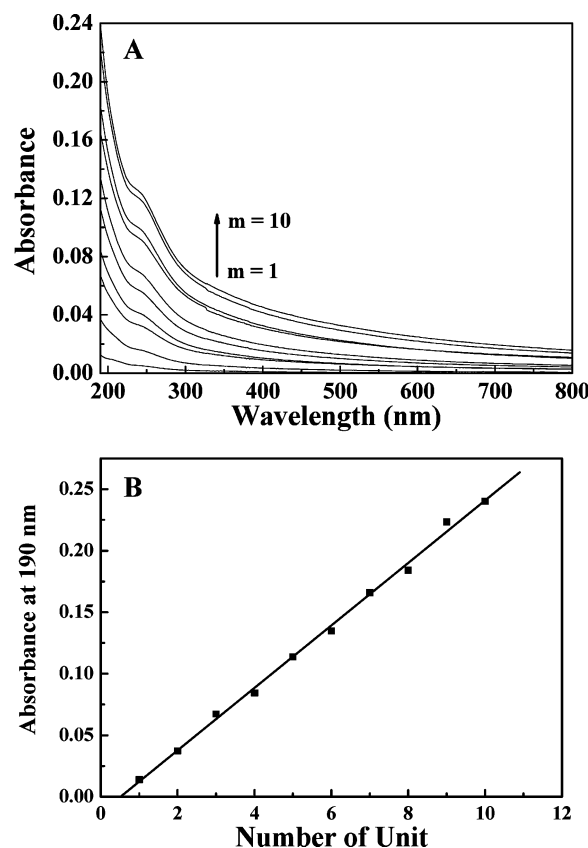


Figure 8. (A) UV absorption spectra of $(\text{PVA}/\text{MMT}/\text{PVA}/\text{LDH})_m$ films. The number of bilayers is 1 through 10 from the bottom to the top [a $(\text{PVA}/\text{MMT}/\text{PVA}/\text{LDH})$ unit is defined as two bilayers of (PVA/MMT) and (PVA/LDH)]. (B) Absorbance at 190 nm is plotted against the number of deposition cycles.

3.3. Layer-by-Layer Assembly of Multilayer Composite Films. The multilayer deposition process was monitored by UV-visible spectroscopy (Figure 8A). A deposited cycle of $(\text{PVA}/\text{MMT}/\text{PVA}/\text{LDH})_m$ was defined as a unit or two bilayers of $(\text{PVA}/\text{MMT})_n$ and $(\text{PVA}/\text{LDH})_n$ (here, $n = m/2$). The absorbance of multilayer films was typically measured after the deposition of each cycle. Absorbance at 190 nm is plotted against the number of deposition cycles (Figure 8B). At this wavelength, the ultrathin films exhibit a strong absorption band. The linear relationship observed between the absorbance and the number of deposited cycle indicates that the deposition process in all cases is reproducible from unit to unit. In other words, for each bilayer system, the amounts of PVA and inorganic blocks adsorbed in each bilayer cycle are the same. These results clearly demonstrate that the layer-by-layer self-assembly process can be successfully carried out with alternative deposition of PVA and inorganic nanosheet. After the deposition of 10 units, the absorbance at 193 nm was 0.24, as indicated in Figure 8B.

Hydrogen-bonding interactions between inorganic nanosheets and PVA drive the reproducible layer-by-layer polymer deposition. PVA is an uncharged, water-soluble polymer. In each unit of PVA, the carbon-bound hydroxyl group can associate with the silicon-bound surface hydroxyl group of MMT or the quartz substrate to form hydrogen bonds, just as indicated schematically in Figure 9. Similarly, in LDH nanosheets there are hydroxyl groups that can associate with PVA or the quartz substrate to form hydrogen bonds, also as demonstrated in Figure 9. Therefore, PVA can ensure the formation of hydrogen bonds between inorganic nanosheet and polymer, which will be

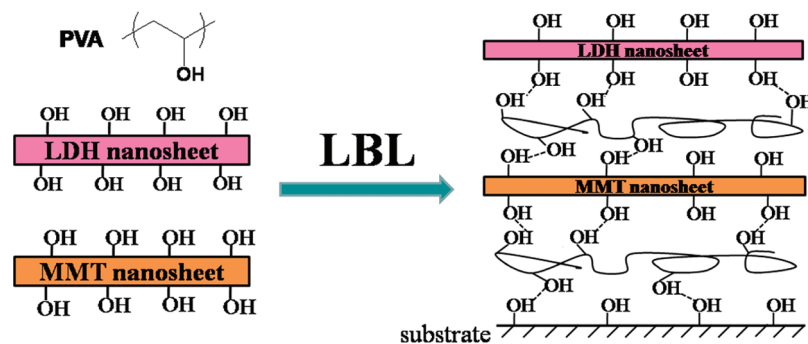


Figure 9. Schematic description of the formation of $(\text{PVA/MMT/PVA/LDH})_m$ film.

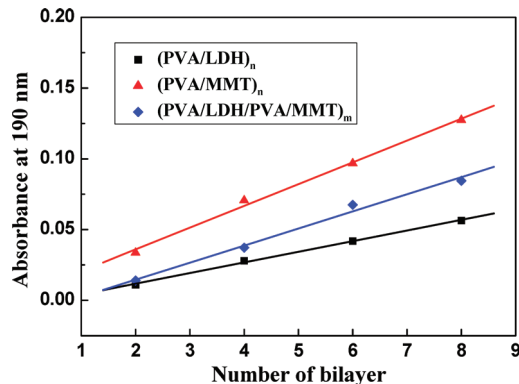


Figure 10. Absorbance at 190 nm is plotted against the number of deposition cycles.

essential to obtain uniform growth of $(\text{PVA/MMT/PVA/LDH})_m$ multilayer films.

Furthermore, $(\text{PVA/LDH})_n$ and $(\text{PVA/MMT})_n$ films were also fabricated through LBL technique. The UV absorption spectra of $(\text{PVA/LDH})_n$ and $(\text{PVA/MMT})_n$ films are illustrated in Figure S2(A) and Figure S3(A), respectively (see the Supporting Information). The absorbance at 190 nm was plotted against the number of deposition cycles for both $(\text{PVA/LDH})_n$ and $(\text{PVA/MMT})_n$ films, as shown in Figure S2(B) and Figure S3(B), respectively (see the Supporting Information). The absorption at 190 nm increases linearly as a function of the number of deposition cycles (Figure 10) for all the three systems investigated above, indicating a stepwise and regular film growth. Compared with the absorption of $(\text{PVA/LDH})_n$ and $(\text{PVA/MMT})_n$ films, $(\text{PVA/MMT/PVA/LDH})_m$ multilayer films exhibit a medium absorption, which further supports the successful LBL assembly process.

The XRD patterns (Figure 11) for the obtained $(\text{PVA/MMT/PVA/LDH})_m$ ultrathin films exhibit a Bragg peak at $2\theta = 4.2^\circ$ and both its intensity and symmetry increase successively upon increasing the deposition cycles. The average thickness of one bilayer is calculated to be about 2 nm (using Bragg equation); therefore, the thickness of one (PVA/MMT/PVA/LDH) unit is about 4 nm. Thus, the thickness of $(\text{PVA/LDH/PVA/MMT})_{10}$ multilayer film is about 40 nm. This diffraction feature can be attributed to the so-called superlattice reflection of the inorganic/organic periodic nanostructure formed by LBL assembly. Similar periodic nanostructures were also reported in the polyelectrolyte/LDH LBL films.^{23,24,26,27}

4. Conclusions

In summary, highly crystalline and monodispersive Co-Al-CO₃ LDH samples were prepared by precipitation through urea hydrolysis under hydrothermal conditions and were

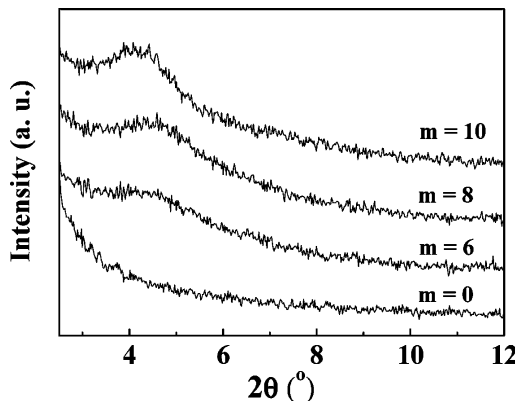


Figure 11. XRD curves of the multilayer films of $(\text{PVA/MMT/PVA/LDH})_m$ assembled on a quartz glass slide.

then delaminated to single layer after decarbonation and anion exchange to Co-Al-NO₃ LDH. After vigorous stirring in water, negatively charged MMT nanosheets were obtained. It is possible that the hydrogen bonding between water and MMT interlayer makes the MMT highly swollen, and this highly swollen phase will then exfoliate into single layers with the assistance of mechanical shearing. LBL technique was used to prepare ultrathin films comprising LDH and MMT nanosheets. PVA as intermediate linkers can ensure the formation of hydrogen bonds between MMT and LDH nanosheets. This hydrogen bonding is essential in order to obtain uniform growth of $(\text{PVA/MMT/PVA/LDH})_m$ multilayer films. Taking the homogeneous ultrathin films with LDH or MMT for comparison, the heterogeneous films are expected to possess a tunable function due to their structural diversity and combined functionality.

Acknowledgment. This work was supported by the National Natural Science Foundation of China (20774019; 50873027), and the Shanghai Leading Academic Discipline Project (Project Number: B113).

Supporting Information Available: SEM image of the Co-Al-Cl LDH sample, UV absorption spectra of $(\text{PVA/LDH})_n$ and $(\text{PVA/MMT})_n$ films, and UV absorbance at 190 nm plotted against the number of deposition cycles. This material is available free of charge via the Internet at <http://pubs.acs.org>.

References and Notes

- Cervilla, A.; Corma, A.; Fornes, V.; Llopis, E.; Palanca, P.; Rey, F.; Ribera, A. *J. Am. Chem. Soc.* **1994**, *116*, 1595.
- Choudary, B. M.; Madhi, S.; Chowdari, N. S.; Kantam, M. L.; Sreedhar, B. *J. Am. Chem. Soc.* **2002**, *124*, 14127.
- Liu, P.; Wang, H.; Feng, Z. C.; Ying, P. L.; Li, C. *J. Catal.* **2008**, *256*, 345.

- (4) Mas, V.; Dieuzeide, M. L.; Jobbagy, M.; Baronetti, G.; Amadeo, N.; Laborde, M. *Catal. Today* **2008**, *133*, 319.
- (5) Wang, Y. F.; Gao, H. Z. *J. Colloid Interface Sci.* **2006**, *301*, 19.
- (6) Olfs, H. W.; Torres-Dorante, L. O.; Eckelt, R.; Kosslick, H. *Appl. Clay Sci.* **2009**, *43*, 459.
- (7) Reinholdt, M. X.; Babu, P. K.; Kirkpatrick, R. J. *J. Phys. Chem. C* **2009**, *113*, 3378.
- (8) Hussein, M. Z. bin; Zainal, Z.; Yahaya, A. H.; Foo, D. W.; V, J. *Controlled Release* **2002**, *82*, 417.
- (9) Tammari, L.; Costantino, U.; Nocchetti, M.; Vittoria, V. *Appl. Clay Sci.* **2009**, *43*, 350.
- (10) Scavetta, E.; Berrettoni, M.; Nobili, F.; Tonelli, D. *Electrochim. Acta* **2005**, *50*, 3305.
- (11) Liu, X. M.; Zhang, Y. H.; Zhang, X. G.; Fu, S. Y. *Electrochim. Acta* **2004**, *49*, 3137.
- (12) Venugopal, B. R.; Ravishankar, N.; Perrey, C. R.; Shivakumara, C.; Raiamathi, M. *J. Phys. Chem. B* **2006**, *110*, 772.
- (13) Su, L. H.; Zhang, X. G.; Liu, Y. *J. Solid State Electrochem.* **2008**, *12*, 1129.
- (14) Lang, K.; Kubat, P.; Mosinger, J.; Bujdak, J.; Hof, M.; Janda, P.; Sykora, J.; Iyi, N. *Phys. Chem. Chem. Phys.* **2008**, *10*, 4429.
- (15) Shi, L.; Li, D. Q.; Wang, J. R.; Li, S. F.; Evans, D. G.; Duan, X. *Clays Clay Miner.* **2005**, *53*, 294.
- (16) Zhang, G.; Ding, P.; Zhang, M.; Qu, B. *J. Polym. Degrad. Stab.* **2007**, *92*, 1715.
- (17) Du, L. C.; Qu, B. *J. J. Mater. Chem.* **2006**, *16*, 1549.
- (18) Peng, H. D.; Tjiu, W. C.; Shen, L.; Huang, S.; He, C. B.; Liu, T. X. *Compos. Sci. Technol.* **2009**, *69*, 991.
- (19) Illaik, A.; Taviot-Gueho, C.; Lavis, J.; Cormereuc, S.; Verney, V.; Leroux, F. *Chem. Mater.* **2008**, *20*, 4854.
- (20) O'Leary, S.; O'Hare, D.; Seeley, G. *Chem. Commun.* **2002**, *14*, 1506.
- (21) Hibino, T.; Jones, W. *J. Mater. Chem.* **2001**, *11*, 1321.
- (22) Adachi-Pagano, M.; Forano, C.; Besse, J. P. *Chem. Commun.* **2000**, *1*, 91.
- (23) Li, L.; Ma, R. Z.; Ebina, Y.; Iyi, N.; Sasaki, T. *Chem. Mater.* **2005**, *17*, 4386.
- (24) Liu, Z. P.; Ma, R. Z.; Osada, M.; Iyi, N.; Ebina, Y.; Takada, K.; Sasaki, T. *J. Am. Chem. Soc.* **2006**, *128*, 4872.
- (25) Li, L.; Ma, R. Z.; Ebina, Y.; Fukuda, K.; Takada, K.; Sasaki, T. *J. Am. Chem. Soc.* **2007**, *129*, 8000.
- (26) Han, J. B.; Lu, J. J.; Wei, M.; Wang, Z. L.; Duan, X. *Chem. Commun.* **2008**, *41*, 5188.
- (27) Yan, D. P.; Lu, J.; Wei, M.; Han, J. B.; Ma, J.; Li, F.; Evans, D. G.; Duan, X. *Angew. Chem., Int. Ed.* **2009**, *48*, 3073.
- (28) Stockton, W. B.; Rubner, M. F. *Macromolecules* **1997**, *30*, 2717.
- (29) Wang, L. Y.; Wang, Z. Q.; Zhang, X.; Shen, J. C.; Chi, L. F.; Fuchs, H. *Macromol. Rapid Commun.* **1997**, *18*, 509.
- (30) Hao, E.; Lian, T. *Langmuir* **2000**, *16*, 7879.
- (31) Zhou, M.; Liu, X.; Zhang, B.; Zhu, H. *Langmuir* **2008**, *24*, 11942.
- (32) Podsiadlo, P.; Kaushik, A. K.; Arruda, E. M.; Waas, A. M.; Shim, B. S.; Xu, J.; Nandivada, H.; Pumplin, B. G.; Lahann, J.; Ramamoorthy, A.; Kotov, N. A. *Science* **2007**, *318*, 80.
- (33) Podsiadlo, P.; Kaushik, A. K.; Shim, B. S.; Agarwal, A.; Tang, Z. Y.; Waas, A. M.; Arruda, E. M.; Kotov, N. A. *J. Phys. Chem. B* **2008**, *112*, 14359.
- (34) MacEwan, D. M. C.; Wilson, M. J. *Interlayer and Intercalation Complexes of Clay Minerals In Crystal Structures of Clay Minerals and Their X-ray Identification*; Brindley, G. W., Brown, G., Eds.; Mineralogical Society: London, 1980.
- (35) Omomo, Y.; Sasaki, T.; Wang, L.; Watanabe, M. *J. Am. Chem. Soc.* **2003**, *125*, 3568.
- (36) Hensen, E. J. M.; Smit, B. *J. Phys. Chem. B* **2002**, *106*, 12664.
- (37) Tambach, T. J.; Hensen, E. J. M.; Smit, B. *J. Phys. Chem. B* **2004**, *108*, 7586.
- (38) Leng, Y. S.; Cummings, P. T. *J. Chem. Phys.* **2006**, *125*, 104701.
- (39) Tambach, T. J.; Bolhuis, P. G.; Hensen, E. J. M.; Smit, B. *Langmuir* **2006**, *22*, 1223.
- (40) Marry, V.; Rotenberg, B.; Turq, P. *Phys. Chem. Chem. Phys.* **2008**, *10*, 4802.

JP907784K